Journal of Polymer Research (2022) 29: 190
https://doi.org/10.1007/s10965-022-03034-1

ORIGINAL PAPER

Synthesis, structural characterization, therotical and electrical properties of novel sulpho-coumarin based methacrylate polymer

Mücahit Özdemir[1] · Fatih Biryan[2] · Kenan Koran[2] · Bahattin Yalçın[1] · Ahmet Orhan Görgülü[1]

Received: 31 January 2022 / Accepted: 14 April 2022 / Published online: 30 April 2022

Abstract

In this study, a new coumarin-based methacrylate monomer was synthesized and its homopolymer P(SCou) was prepared by free radical polymerization method. The structural characterization of the compounds was performed by using FT-IR, ^{1}H and ^{13}C-NMR spectroscopic techniques. The thermal behavior of the polymer was investigated by differential scanning calorimetry (DSC) and thermogravimetric analysis (TGA) methods. Thermal decomposition kinetics were investigated with TGA results at different heating rates by non-isothermal method. Thermal decomposition activation energy of homopolymer was calculated according to Flynn–Wall–Ozawa in the 5%-50% conversion range. The average activation energy of P(SCou) was found to be 220.21 kJ/mol. Theoretical calculations were done with Gaussian and the results were visualized with GaussView 5.0 and IQMol. Geometry optimizations of sulfocoumarin monomer and polymer were calculated with Becke-3-Lee–Yang–Parr's functional correlation (B3LYP). Optical band gaps for sulfonyl coumarin-(SCou), its monomer SCou-MA and P(SCou) compounds are 3.615, 3.723 and 3.792 eV, respectively. The dielectric properties of the polymer were investigated as a function of frequency and temperature in the frequency range of 1–200 kHz. Also, a heterojunction Shotky diode of the polymer was prepared on a p-type Si substrate using the thin-film technique. The I-V characteristic of the polymer/p-Si thin film heterojunction diode was determined between ± 4 V and the various illumination intensities. The device has displayed good rectification behavior proving the creation of Schottky junction. The ideality factor was determined as 3.71, and the reverse supply current was determined as 8.78×10^{-5} A.

Keywords Coumarin · Homopolymer · Therotical properties · Electrical properties · Diode

Introduction

In recent years, the use of organic compounds, which have more favorable and more promising properties for many application areas, instead of traditionally known inorganic semiconductor materials, has attracted the attention of researchers [1]. These organic materials and their derivatives have mostly been studied in different device formats such as Schottky diodes, organic light-emitting diodes, organic field-effect transistors, photovoltaic (PV) and solar cells [2–8]. Coumarins are organic heterocyclic compounds known as benzopyrans, formed as a result of the coordination of the pyran ring and the benzene ring. Due to their unique properties, coumarins have attracted interest in research studies [9–11]. However, coumarin derivatives are colorless and exhibit intense fluorescence and absorption spectra with a high quantum yield in the visible range [12–14]. In addition, coumarins can be used in versatile scientific and technological applications such as photonics and optoelectronics, organic light-emitting diodes and solar cells, due to their easy synthesis, high efficiency, good solubility and excellent photostability [15–18]. The optical properties of the coumarin molecule change when a functional group is added. The type of functional group, whether it is an electron donor or acceptor, electron delocalization and hence electron mobility plays a very important role in the molecular structure of coumarin [19–21].

Functional polymers have attracted great commercial and scientific interest due to their potential and promising applications in many fields such as energy, biosensors and high performance materials. Functional polymers can prepared

✉ Fatih Biryan
fbiryan@firat.edu.tr

[1] Department of Chemistry, Marmara University, 34722, Kadikoy, Istanbul, Turkey

[2] Faculty of Science, Department of Chemistry, Fırat University, 23169 Elazig, Turkey

by polymerization of monomers obtained as a result of chemical modification of desired groups [22, 23]. Due to the increasing need for advanced technological materials with different properties, studies on the synthesis of new functional polymers and determination of application areas continue [24–28]. Acrylate and methacrylate derivatives are the most widely used ways in polymerization to increase the functionality of functional polymers. The wide range of applications of acrylate and methacrylate-containing monomers and polymers has attracted the attention of scientists [29, 30]. Methacrylate monomers provide high light transmittance due to their optical transparency. In addition, their high mechanical and thermal durability allows them to be used in a wide range of applications [31].

Although there are few studies on the electrical properties of coumarin compounds, the synthesis, thermal and electrical properties of the methacrylate polymer bearing coumarin side chains containing sulfonyl groups have not been encountered. In this study, a new coumarin-based methacrylate monomer was synthesized and its homopolymer was prepared by free radical polymerization method in presence of AIBN. The thermal behavior of the polymer was investigated by differential scanning calorimetry (DSC) and thermogravimetric analysis (TGA) methods. Thermal decomposition kinetics were investigated with TGA results measured at different heating rates by non-isothermal method. Thermal decomposition activation energy of homopolymer was calculated according to Flynn–Wall–Ozawa in the 5%-50% conversion range. Theoretical calculations were done with Gaussian and the results were visualized with GaussView 5.0 and IQMol. Geometry optimizations of sulfocoumarin monomer and polymer were calculated with Becke-3-Lee–Yang–Parr's functional correlation (B3LYP) The dielectric properties of the polymer were investigated as a function of frequency and temperature in the frequency range of 1–200 kHz. Also, a heterojunction Shotky diode of the polymer was prepared on a p-type Si substrate using the thin-film technique. The I-V characteristic of the polymer/p-Si thin film heterojunction diode was determined between ± 4 V and the various illumination intensities.

Experimental

Materials

2,4-dihydroxybenzaldehyde, 4-methylsulfonyl)phenylacetic acid, sodium acetate, dry acetic anhydride, methacryloyl chloride and triethylamine were kindly provided by Sigma-Aldrich and used as received. All of the other materials used were of analytical purity and were used as commercially received.

Characterization techniques

The NMR spectra of samples were recorded by 400 MHz Bruker AVANCE III NMR spec-trometer. FT-IR spectra of the pecimens that are in the powder form has been recorded by using the Attenuated Total Reflection (ATR) unit of the Thermo Nikolet IS5 spectrometer in the 400–4000 cm $^{-1}$ range. A background cancelation was in session after every reading and the spectra have been obtained at the end of 16 successive reading. Thermogravimetry (TG) measurements were carried out using a Shimadzu DTG-60 model thermogravimetric analyzer under nitrogen flow (10 mL/min) from 25 to 600 °C at heating rate of 10 °C /min. The current–voltage(I-V) and capacitance–voltage (C-V) measurements were taken using FYtronic Electric Characterization system carried out in the dark. Optical spectra in the UV–vis region were recorded with a Shimadzu 2450 UV–vis spectrophotometer. Fluorescence excitation and emission spectra were recorded on the Hitachi F-7000 spectro fluorometer using 1 cm path length cuvette at room temperature.

7-Hydroxy-3-[4-(methylsulfonyl)phenyl]-coumarin synthesis

2.00 g (14.48 mmol) 2,4-dihydroxybenzaldehyde, 3.10 g (14.48 mmol) 4-methylsulfonyl)phenylacetic acid and 1.78 g (21.72 mmol) sodium acetate were dissolved in 15 mL dry acetic anhydride and heated 160 °C under N_2 atmosphere for 22 h. The reaction product was precipitated in ice water and filtered. The crude product containing acetyl group was dissolved in 100 mL MeOH/THF (3:1) and 1.00 g (41.75 mmol) LiOH solution dissolved in 5 mL of water was added to the reaction. After 3 h, the reaction mixture was precipitated into acidic ice water. The precipitate was filtered by filtration and dried. The crude product was purified by crystallization in methanol. Yield 3.75 g (81.87%). Synthesis reaction of SCou is shown in Scheme 1.

The FT-IR spectrum of SCou is shown in Fig. 1.

FT-IR (ATR, υ_{max}, cm^{-1}): 3281 (–OH), 3063–3025 (Ar–C–H), 2996–2924(Aliphatic-C–H), 1723 and 1671 (–C = O), 1608–1589 (Ar–C = C).

The ^{1}H and ^{13}C-NMR spectra of SCou are shown in Fig. 2a and b, respectively.

^{1}H-NMR (400 MHz, DMSO-d_6): δ_H, ppm: 10.76 (1H, **H^{1}**), 8.34 (1H, **H^{8}**), 7.99 (4H, **H^{12}-H^{13}**), 7.66–7.63 (1H, **H^{4}**), 6.87–6.85 (1H, **H^{3}**), 6.76 (1H, **H^{7}**), 3.26 (3H, **H^{15}**).

^{13}C-NMR (400 MHz, DMSO-d_6): δ_C, ppm: 162.40 (**C^{10}**), 160.23 (**C^{3}**), 155.77 (**C^{6}**), 143.25 (**C^{8}**), 140.68 (**C^{11}**), 140.34 (**C^{14}**), 130.95 (**C^{4}**), 129.52 (**C^{13}**), 127.31 (**C^{12}**), 120.89 (**C^{9}**), 114.14 (**C^{3}**), 112.29 (**C^{5}**), 102.28 (**C^{7}**), 044.01 (**C^{15}**) Scheme 1.

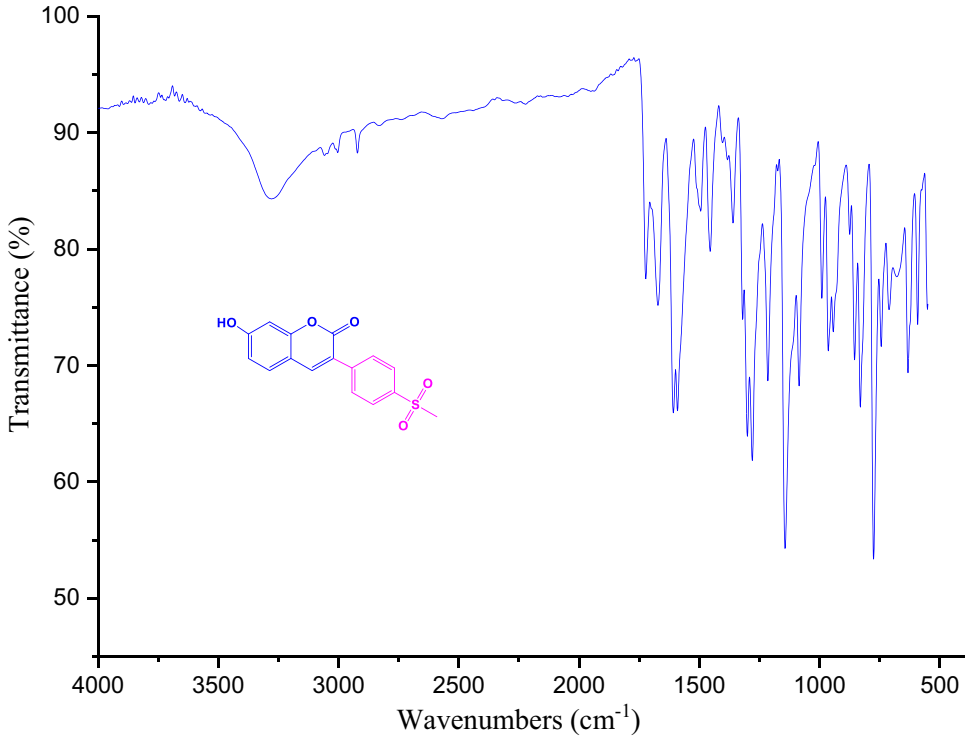

Fig. 1 FT-IR spectrum of SCou (ATR)

SCou-MA monomer synthesis

1 g (3.16 mmol) SCou was dissolved in THF and 0.363 g (3.48 mmol) triethylamine was added in the reaction flask. After cooling the solution temperature to 0–5 °C with an ice bath, 0.351 g (3.48 mmol) methacryloyl chloride added dropwise in the reaction for 20 min. After 12 h, the reaction was stopped and the salt formed was filtered and precipitated in water after removing some of the solvent. The product was filtered as white solid and dried at 30 °C under vacuum. The yield of the monomer was calculated as 82%. Synthesis reaction of SCou-MA is shown in Scheme 2.

The FT-IR spectrum of SCou-MA is shown in Fig. 3.The important signals for structure of monomer are summarized following as:

FT-IR (ATR, υ_{max}, cm^{-1}): 3063–3011 (Ar–C–H), 2976–2926 (Aliphatic-C–H), 1726 and 1697 (–C = O), 1632 (C = C in viniyl group), 1613–1591 (Ar–C = C).

The ^{1}H and ^{13}C-NMR spectra of SCou-MA are shown in Fig. 4a and b, respectively.

^{1}H-NMR (DMSO-d_6, δppm): 2.03 (3H, **H^{17}**), 3.28 (3H, **H^{14}**), 5.98 and 6.35 (cis (**H^{20}**) and trans (**H^{19}**) proton respectively on vinyl group), 7.27 (1H, **H^{2}**), 7.44 (1H, **H^{6}**), 7.89 (1H, **H^{3}**), 8.02–8.01 (4H, **H^{11}-H^{12}**), 8.44 (1H, **H^{7}**).

^{13}C-NMR (DMSO-d_6, δppm): 18.49 and 43.95 (methyl carbons, **C17** and **C14**), 110.41 (**C6**), 117.72 (**C4**), 119.50 (**C2**), 125.25 (**C8**), 127.38 (**C11**), 129.01 (**C18**), 129.89 (**C12**), 130.38 (**C3**), 135.39 (**C16**), 140.11 (**C10**), 140.93 (**C13**), 142.26 (**C7**), 153.79 (**C1**), 154.26 (**C5**), 159.71 (**C9**), 165.61 (**C15**).

Free radical polimerization of SCou-MA

SCou-MA monomer was polymerized by free radical polymerization method at 60 °C in the presence of 1,4-dioxane using AIBN as initiator. The obtained polymer was precipitated by dropwise transfer to ethanol. The polymer was dissolved in tetrahydrofuran and a second precipitation was made in ethanol then dried under vacuum at 40 °C for 12 h. Synthesis reaction of P(SCou) is shown in Scheme 3.

The FT-IR spectrum of P(SCou) is shown in Fig. 5, and it represented the important signals such as (υmax, cm^{-1}): 1725 (ester carbonyl), 1610 (carbonyl on coumarin) and 1350–1307 (S = O stretching).

^{1}H-NMR spectrum was given in Fig. 6a. The characteristic signals of polymer were summarized for as follows: (DMSO-d_6, δppm): 8.39–7.18 (8H, aromatic ring protons), 3.34 (methyl protons on the side chain), 1.30 and 0.90 (main chain protons).

^{13}C-NMR spectrum was given in Fig. 6b.^{13}C-APT NMR (DMSO-d_6, δppm): 18.49 and 43.88 (methyl carbons), 24.47–25.04 (main chain carbons), 159.46 (carbonyl carbon on coumarin), 165.32 (carbonyl carbon on methacrylate).

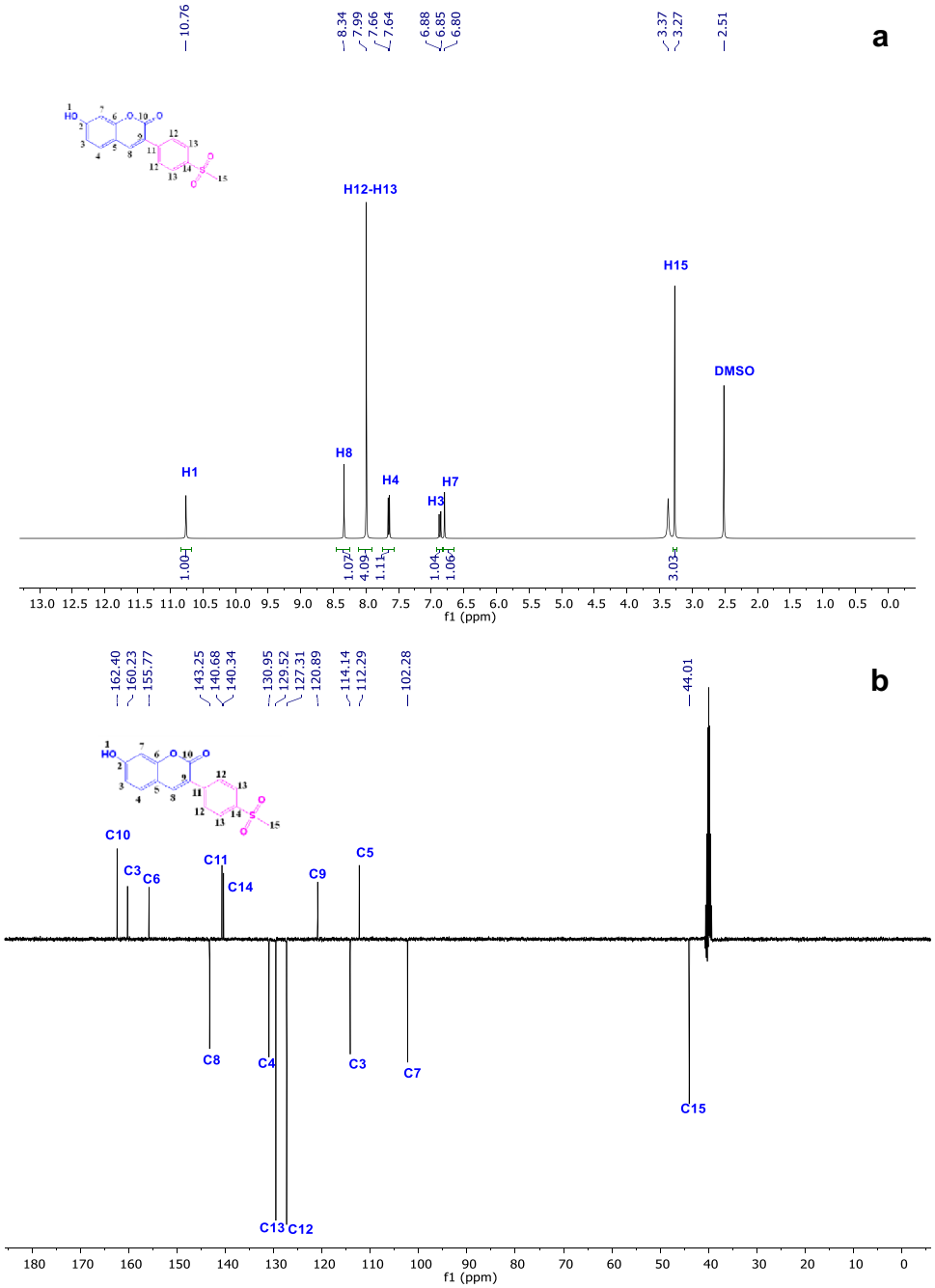

Fig. 2 **(a)** ^{1}H-NMR and **(b)** ^{13}C-NMR spectra of SCou (DMSO-d_6)

In the FT-IR spectrum of the homopolymer, the C = C stretching vibration belonging to the vinyl group in the monomer disappeared. In addition, the olefinic protons of the monomer at 5.98 and 6.35 in the H-NMR spectrum of the homopolymer were disappeared. These protons were observed as main chain protons in the range of 0.9–1.40 ppm.

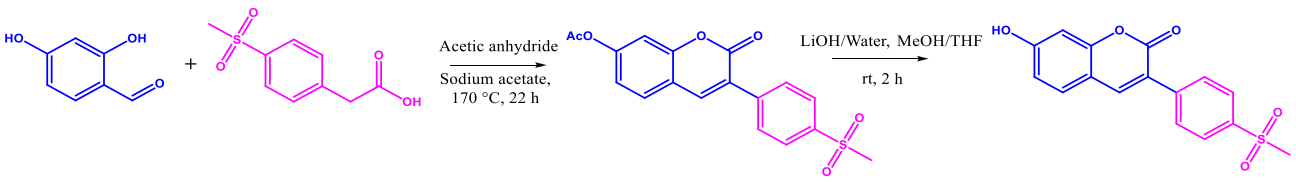

Scheme 1 Synthesis of SCou

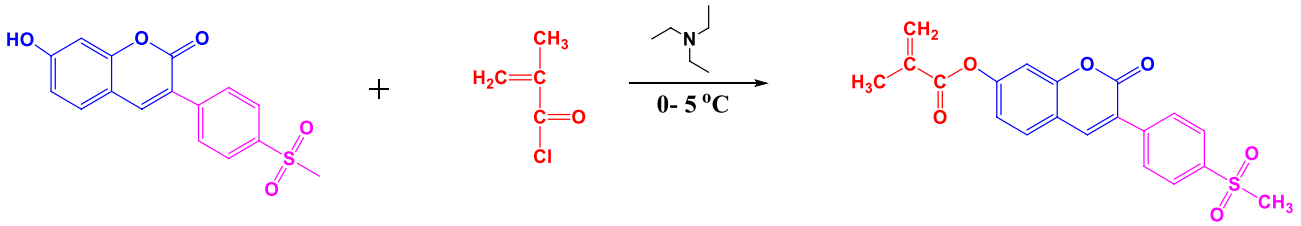

Scheme 2 Synthesis of SCou-MA monomer

Results and discussion

Thermal characterization

The glass transition temperature, which is a characteristic value for polymers, is known as the temperature at which the polymer becomes hard and brittle when cooled after heating. Therefore, it is important to determine the glass transition temperature in the investigation of the thermal behavior of newly synthesized polymers. At the glass transition temperature, the weak secondary bonds that bind the polymer chains together are broken and the macromolecule begins to form.

DSC analysis was performed under nitrogen atmosphere from ambient temperature to 200 °C at a heating rate of 20 °C min^{-1}. DSC curve of P(SCou) is shown in Fig. 7. The glass transition temperature was determined as 122 °C. This temperature is considerably higher than some methacrylate polymer in the literature [32, 33]. This is thought to be due to the presence of the coumarin group, which is a hard and bulky structure, in the side chain of the homopolymer. The glass transition temperature of amorphous polymers is related to the chain flexibility. This value is characteristic for understanding the chain mobility of polymers. Coumarin and sulfo groups in the structure of P(SCou) decrease polymer chain flexibility and increase Tg.

In Fig. 8a the non-isothermal TGA curves of the P(SCou) homopolymer are shown comparatively. TGA analyzes were carried out at different heating rates of 5, 10, 20, 30 and 40 °C/min in nitrogen atmosphere from room temperature to 600 °C and with approximately 5 mg sample. Figure 8a shows the non-isothermal TG curves and as a comparison to that of P(SCou). Decomposition of P(SCou) was found to occur in two stages. The initial and fnal degradation temperatures are: 326–424 °C for the frst stage, and 462–560 °C for the second stage. There are two different methods known as model fitting and model-free for the analysis of kinetic data obtained from TGA measurements. Flynn–Wall–Ozawa which is a model-free method, was used

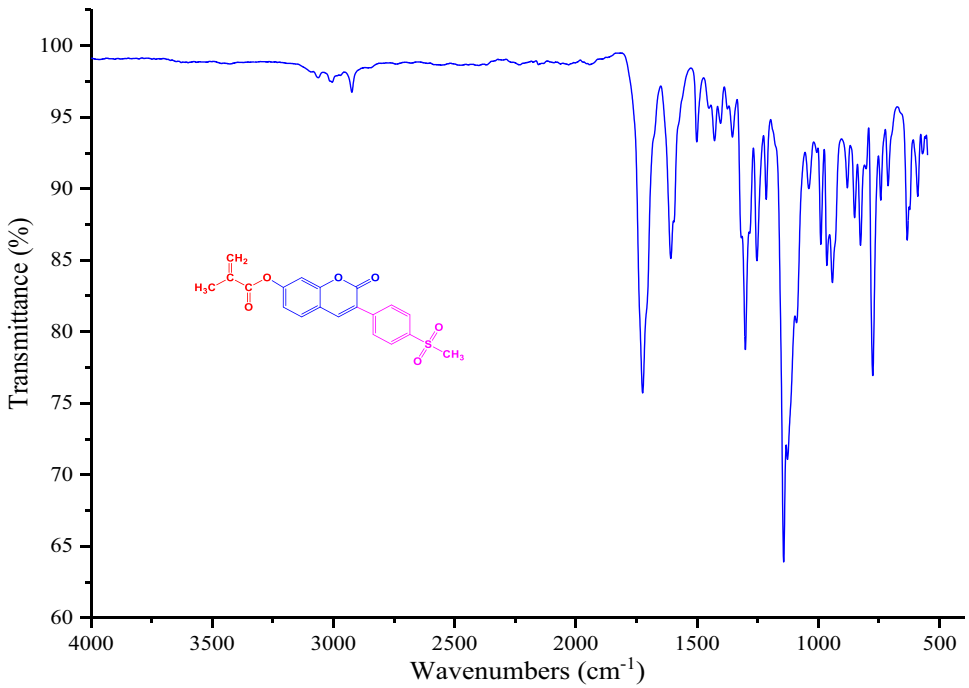

Fig. 3 FT-IR spectrum of SCou-MA monomer (ATR)

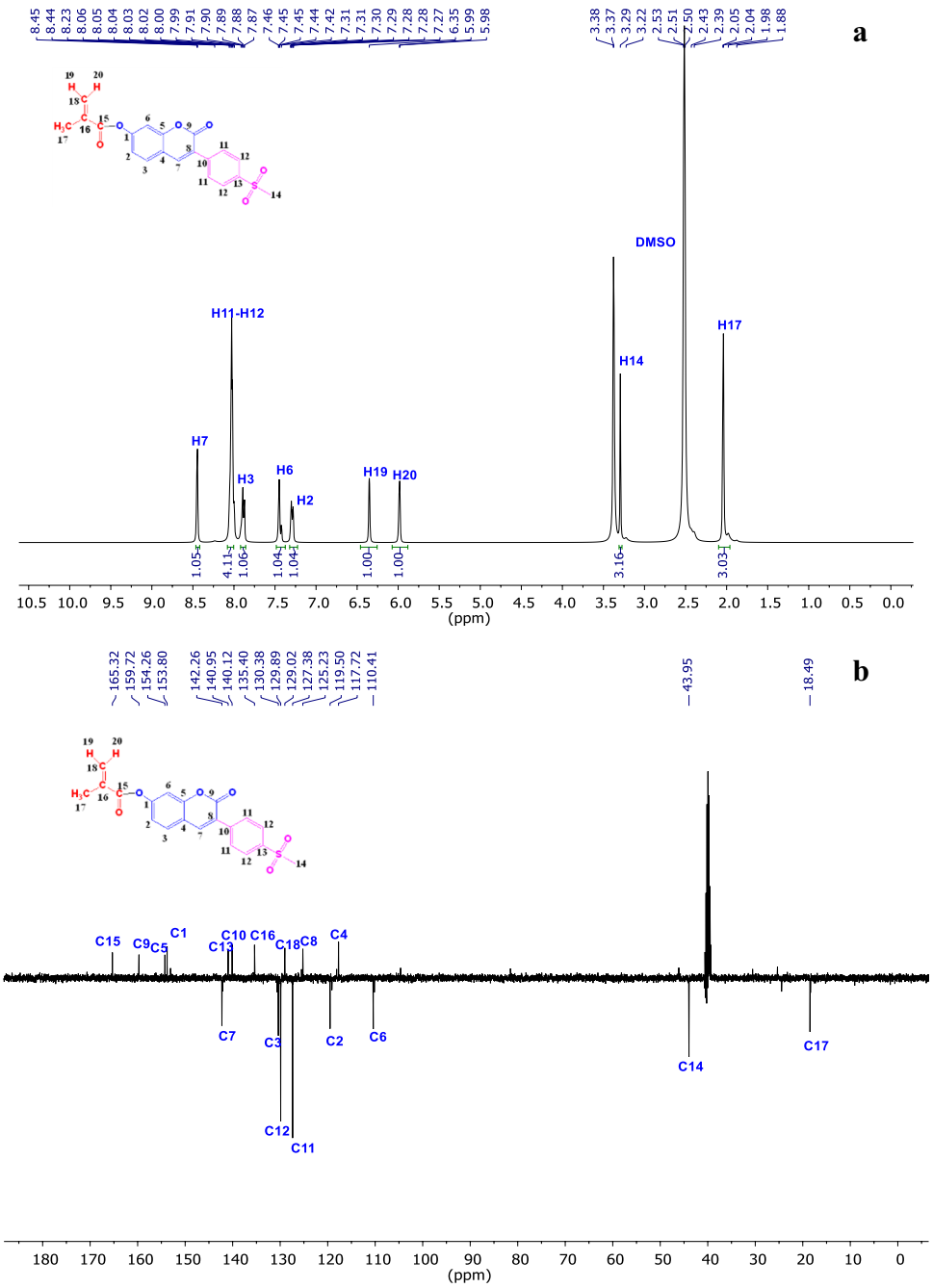

Fig. 4 **(a)** ^{1}H-NMR and **(b)** ^{13}C-NMR spectra of SCou-MA monomer (DMSO-d_6)

to determine the thermal decomposition activation energy of SCou homopolymer [34, 35]. FWO curves were obtained by using the temperature values obtained from different heating rates in the 5%-50% conversion range of P(SCou). Activation energies corresponding to the 5%-50% conversion range for the homopolymer were calculated from the slope of the lnβ lines versus the 1/T curves shown in Fig. 8b. According to these results, the average activation energy of P(SCou) was found to be 220.21 kJ/mol at 0.50 conversion. This value is higher than the activation energy of the methacrylate polymer containing chalcone group determined according to the Flynn–Wall–Ozawa method in the literature [36]. The activation energy obtained from the TGA analysis is determined depending on the mass loss during decomposition [37]. It was also observed that the activation energy showed an increasing–decreasing effect with extent of conversion. Generally, there is an increase in activation energy due to degradation. It can be observed, the activation energy for 0.3 conversion is maximum value. The change of activation energy depending on the conversion degree is shown in Fig. 9. At the initial values of the convertion, the activation energy was determined as minimum. Activation

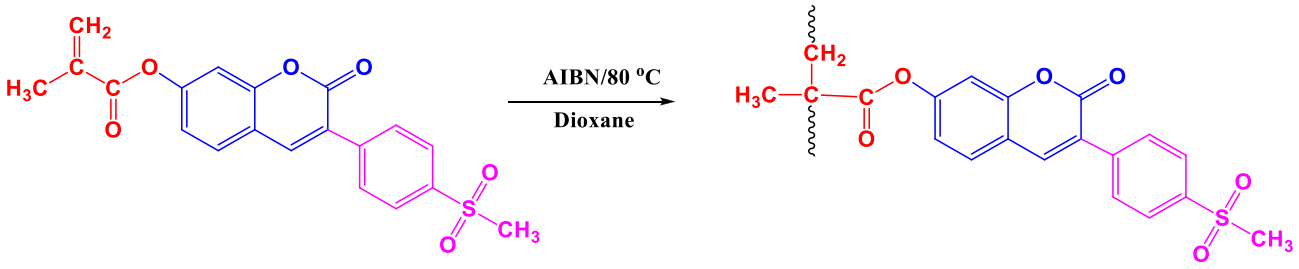

Scheme 3 Synthesis of P(SCou)

energy is low in the frst phase of the conversion because of the elimination of evaporating contents and breaking of weaker bonds [38]. High values in activation energy can be attributed to the depolymerization that occurs in the polymer under dynamic heating conditions [39].

Theoretical calculations

Theoretical calculations were done with Gaussian 09 [40], and the results were visualized with GaussView 5.0 [41] and IQMol. Geometry optimizations of sulfocoumarin (SCou), monomer-sulfocoumarin SCou-MA and polymer sulfocoumarins P($SCou_{n=2-6}$) were calculated with Becke-3-Lee–Yang–Parr's functional correlation (B3LYP) [42–44] of 6-31G(d,p) level of theory in the density functional theory. Frequency studies were done in addition to geometry optimization and compared to experimental data. Electrostatic potential measurements were used to compute the total electron density surface. SCF/ESP was used as the density matrix to display the whole electron surface. The Polarizable Continuum Model (PCM) [45, 46] in the ground state, as implemented in Gaussian09, was used to explore the solvent impact. The time-dependent DFT approach was used to detect UV–Vis absorption and fluorescence emission spectra in chloroform to compare experimental and theoretical absorption and emission spectra.

Ground state electronic absorption and fluorescence spectra

Coumarins can be characterized by UV–Vis and Fluorescence spectroscopy due to their emission and absorption in the UV visible region. The characteristic bands of coumarins are generally observed in the viole region (300–400 nm). Sulfocoumarin SCou, monomer SCou-MA and polymer Poly(SCou) samples were measured in chloroform. Absorption bands were observed at 343 nm ($\log\varepsilon = 4.88$) for sulfocoumarin SCou and 333 nm

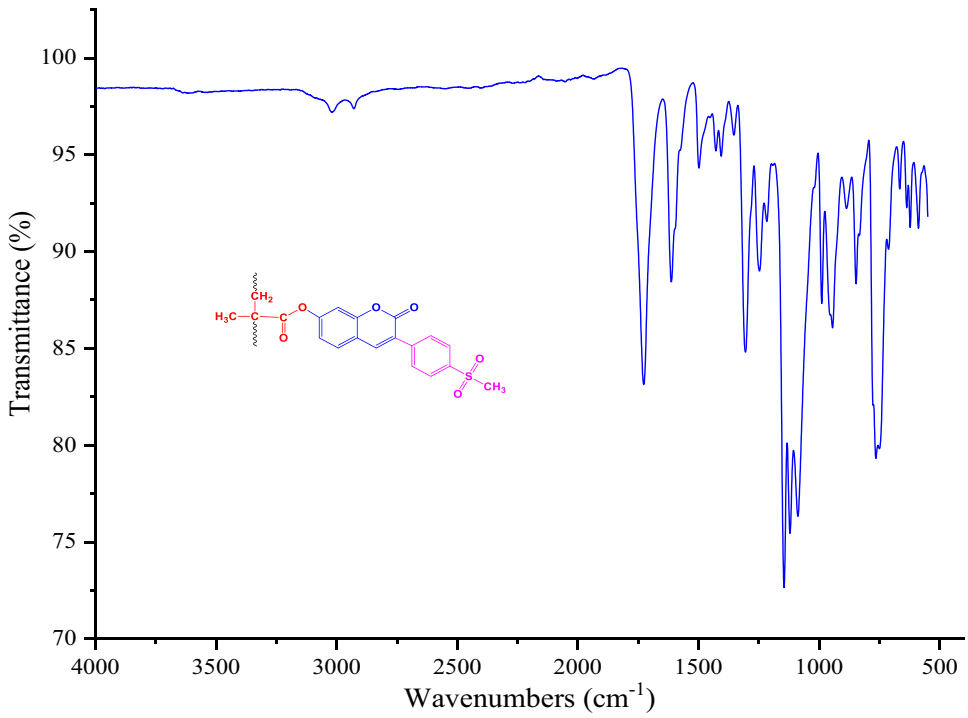

Fig. 5 FT-IR spectrum of P(SCou) (ATR)

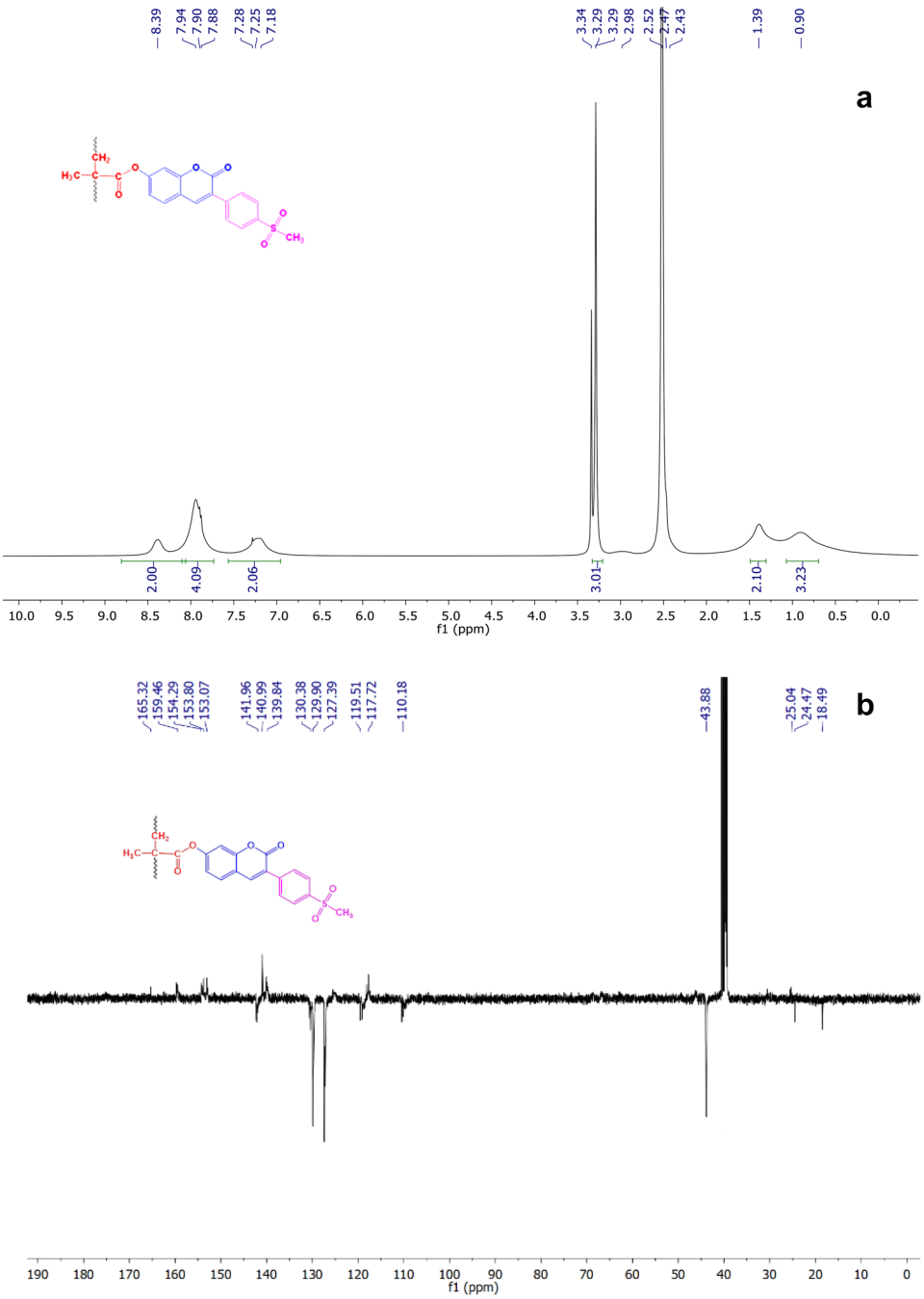

Fig. 6 **(a)** ^{1}H-NMR and **(b)** ^{13}C-NMR spectra of P(SCou) (DMSO-d_6)

(logε = 4.89) for monomer-sulfocoumarin SCou-MA at 327 nm (logε = 4.94) for polymer sulfocoumarin. The UV of the hydroxy coumarin compound shifted to 10 nmblue with the addition of the methacrylate group in the monomer. The homopolymer obtained by polymerization of the monomer shifted to 6 nm blue. The reason for the blue shift is the hydrogen bond molecular interactions between the monomers in the polymer structure [47].

Sulfocoumarin (SCou), monomer-sulfocoumarin SCou-MA and polymer sulfocoumarin (Poly-SCou) compounds have high fluorescence emission in chloroform. The emission bands of coumarins were observed at 433 nm (λ^{em}_{start} = 343 nm) for (SCou), 413 nm (λ^{em}_{start} = 333 nm) for SCou-MA and 411 nm (logε = 4.94) for P(SCou). There are 6060, 5817 and 6216 cm-1 stokes shifts between emission and absorption bands of sulfocoumarin (SCou), monomer-sulfocoumarin SCou-MA and polymer sulfocoumarins, respectively. The Stokes shift was decreased when the methacrylate group was added to coumarin because the hydroxyl (–OH) is a donor group. In addition, the hydrogen

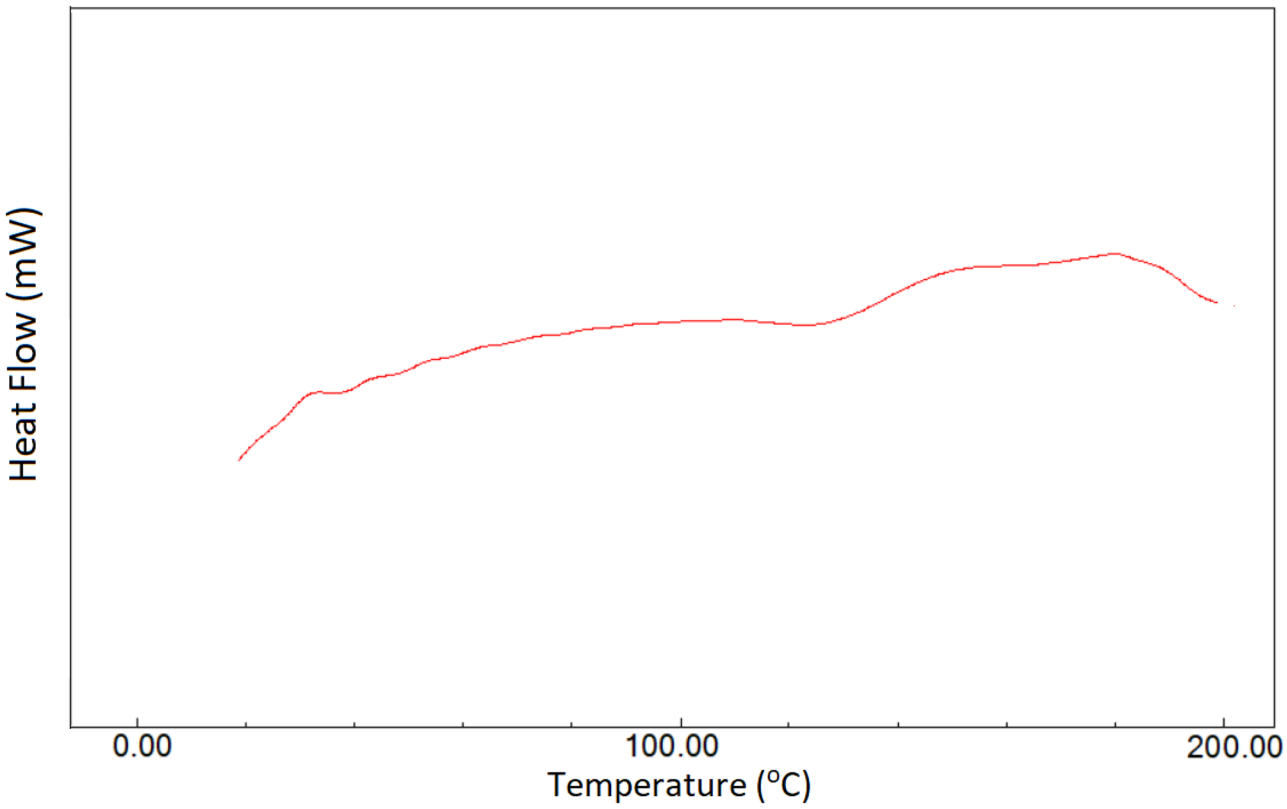

Fig. 7 DSC curve of homopolymer P(SCou)

bond molecular interactions between the monomers in the polymer structure increased the Stokes shift compared to the monomer.

Density functional theory results

Recently, theoretical calculations have become very attractive to study the molecular, electrochemical, thermochemical and spectral properties of compounds. Polarizability (α), HOMO–LUMO, band gap (EGAP), dipole moment (D), ionization potential (IP), electron Affinity (EA), electronegativity (χ), chemical hardness (η), global softness (σ), electrophilicity index (ω) values of Sulfocoumarin (SCou), monomer SCou-MA and (Poly-(SCou n = 2–6) were calculated by DFT method.

The polymer sulfocoumarin compound was optimized to contain di-, tri-, tetra-, penta-, and hexa-monomer and the values were compared among each other. Calculated parameters of all sulfocoumarin forms are shown in Table 1.

Polarizability (α) gives a good idea for the dielectric properties of polymers. Electric fields inside dielectrics polarize the material. Therefore, polarizability is related to the dielectric constant. As the dielectric constant increases, the polarizability also increases. As the number of electrons in the molecule increases, the polarizability increases, but there is a negative correlation between the values of polymers containing n = 3 and 5 monomers, and polymers containing n = 2, 4 and 6 monomers. The reason for this inconsistency is the variable symmetry of the structure and the dipole moment. HOMO (Highest Occupied Molecular Orbital) values of sulfonyl coumarin SCou and its monomer SCou-MA and polymer P(SCou = $_{2–6}$) compounds are close to each other for all compounds (between -6.196 and -6.510 eV)). LUMO (Lowest Unoccupied Molecular Orbital) values decreased in monomer structure compared to sulcoumarin and continued to decrease as the number of monomers in the polymer increased (between -2.225 and -2.919 eV). The band gap of the monomer increased relative to the sulpho-coumarin compound. Band gap decreased as the number of mers in the polymer chain increased. In addition, single mer number polymers have wider band gaps and double mer number polymers have narrower band gap (Fig. 10). The formula $E_g = 1240/\lambda$ (eV) was used while calculating the optical band gaps. Optical band gaps for sulfonyl coumarin-(SCou), its monomer (Mono-SCou) and P(SCou) compounds are 3.615, 3.723 and 3.792 eV, respectively.

The bond polarity of the coumarin derivatives increased with the obtaining of monomer from the sulcoumarin

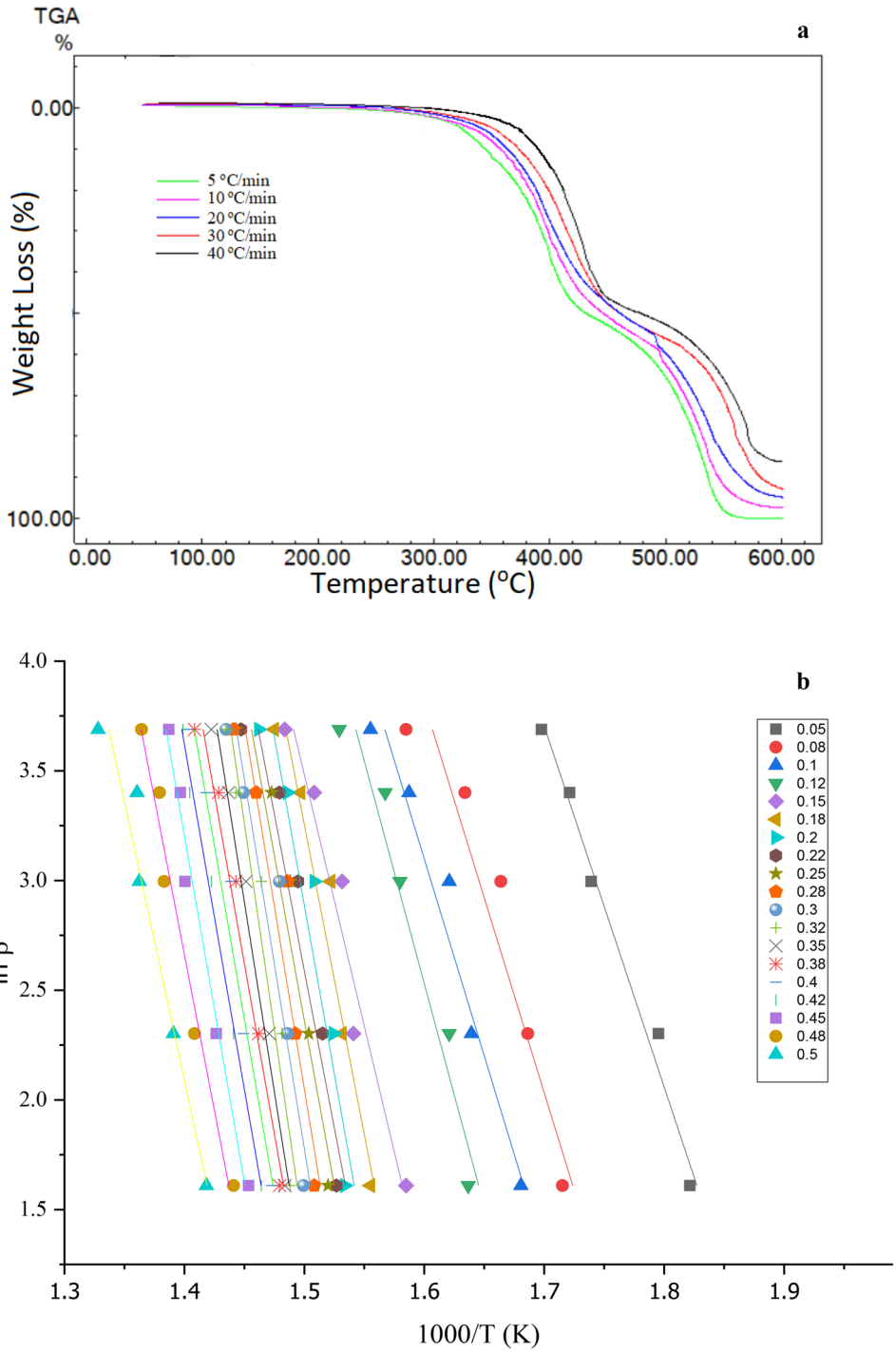

Fig. 8 (**a**) TGA curves in diferent heating rates of P(SCou) (**b**) the results of Flynn–Wall–Ozawa analysis (lnβ vs. 10^3/T)

compound and the polymer number increased when n = 2, 4 and 6, but decreased when n = 3 and 5. The ionization potential (IP), electron affinity (EA), electronegativity (χ), chemical hardness (η) and softness (σ) values for all coumarin compounds are close to each other.

The obtained molecular orbital diagram from DFT of compound are shown in Fig. 11. For the total electron densities of coumarin compounds, the total SCF density (isoval = 0.0004 e/au^3) was calculated and mapped with electrostatic potential (ESP). SCou-MA has a darker electron density map than the SCou compound as a result of the conversion of the electron-donating hydroxy group to ester. The red color symbolizes electronegativity, that is, the substituent in that region is the electron withdrawing group. The green color is neutral and the blue color symbolizes electropositivity, that is, the substituent in that region is the

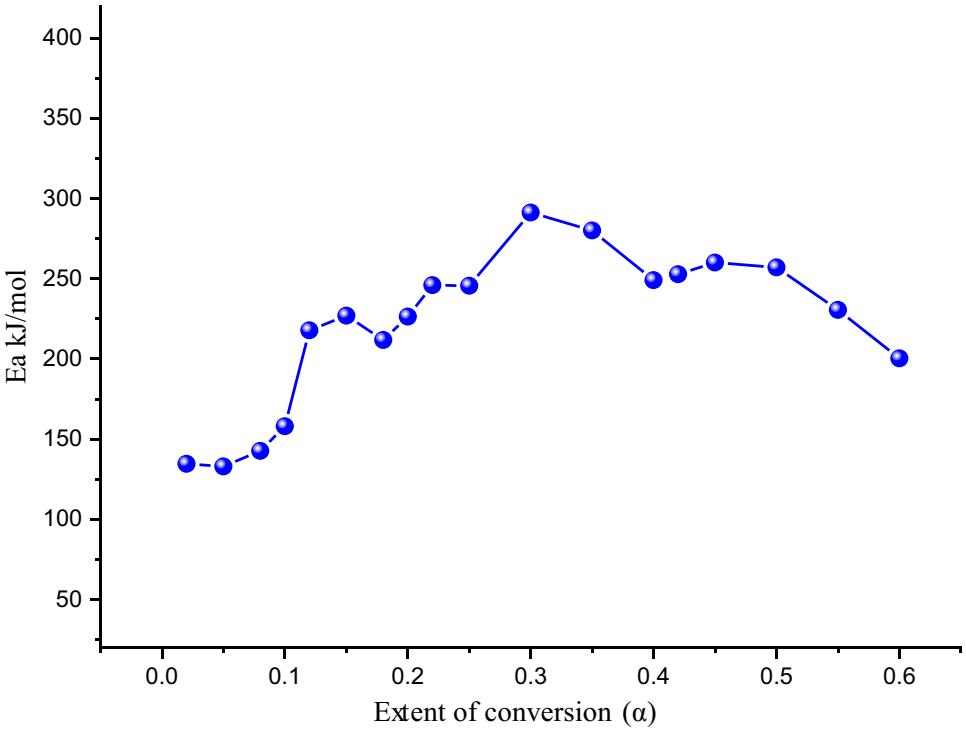

Fig. 9 Comparison of the dependence of Ea on the extent of conversion for P(SCou)

Table 1 The calculated parameters of the (SCou), (SCou-MA) and P($SCou_{n=2-6}$) derivatives using the B3LYP/6-31G (d,p) level of theory, the DFT method

	SCou	Mono-SCou	Poly(SCou)				
			(n = 2)	(n = 3)	(n = 4)	(n = 5)	(n = 6)
Polarizability (α)	225.07	279.81	553.77	818.80	737.69	1361.9	901.10
LUMO + 1 Energy	-0.995	-1.665	-2.404	-2.628	-2.584	-2.814	-2.880
LUMO Energy (E_{LUMO})	-2.225	-2.378	-2.719	-2.815	-2.951	-2.870	-2.919
HOMO Energy (E_{HOMO})	-6.202	-6.390	-6.415	-6.473	-6.307	-6.510	-6.196
HOMO -1 Energy	-7.196	-7.169	-6.785	-6.669	-6.569	-6.515	-6.372
Energy Gap (E_{GAP})	3.977	4.012	3.696	3.658	3.356	3.640	3.277
Dipole Moment (D)	6.990	7.680	11.710	11.540	12.480	10.930	18.980
Ionization Potential (IP)	6.202	6.390	6.415	6.473	6.307	6.510	6.196
Electron Affinity (EA)	2.225	2.378	2.719	2.815	2.951	2.870	2.919
Electronegativity (χ)	4.214	4.384	4.567	4.644	4.629	4.690	4.558
Chemical Hardness (η)	1.989	2.006	1.848	1.829	1.678	1.820	1.639
Global Softness (σ)	1.006	0.997	1.082	1.093	1.192	1.099	1.220
Electrophilicity index (ω)	4.464	4.790	5.643	5.896	6.385	6.043	6.338
$E_{GAP} = E_{HOMO} - E_{LUMO}$	$IP = -E_{HOMO}$			$EA = -E_{LUMO}$		$\chi = (IP + EA)/2$	
$\eta = (IP - EA)/2$	$\sigma = 1/2\eta$			$\omega = \chi^2/2\eta$			

Formula references from [48–54]

The dipole moment unit is Debye (D).

The polarizability unit is Hartree (a.u.)

HOMO and LUMO energy, Energy gap, Electron affinity, Ionization potential, Chemical hardness, Electronegativity, and Electrophilicity index unit are Electron Volt (eV)

The global softness unit is 1 / Electron Volt (eV^{-1})

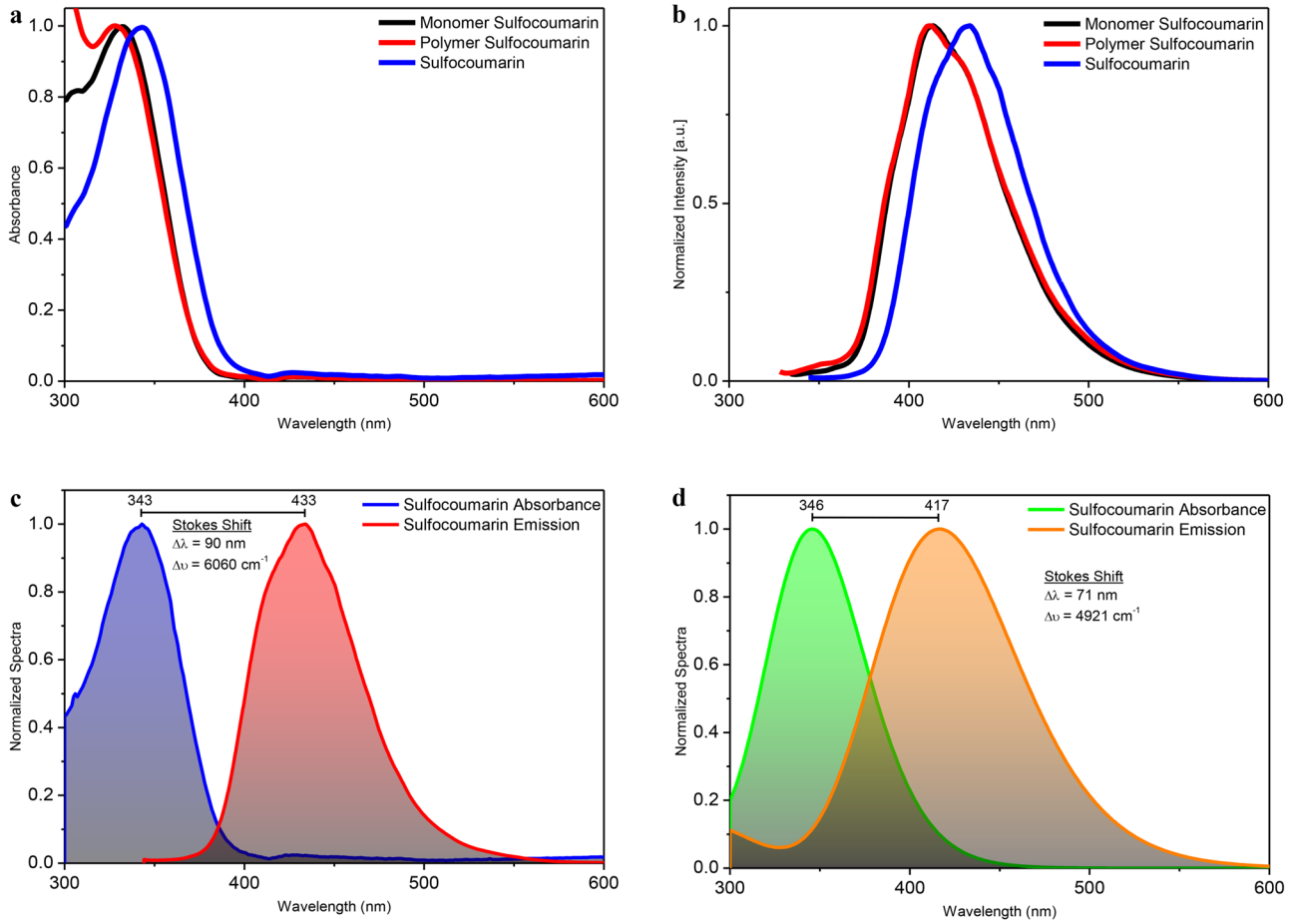

Fig. 10 (**a**) The normalized UV–Vis absorption spectra of sulfocoumarin (SCou), monomer-sulfocoumarin SCou-MA and polymer sulfocoumarins Poly($SCou_{n=2-6}$) in chloroform. (**b**) The normalized fluorescence emission spectra of sulfocoumarin (SCou), monomer-sulfocoumarin SCou-MA and polymer sulfocoumarins Poly($SCou_{n=2-6}$) in chloroform. (**c**) Representation of stokes shift between the experimental absorption and emission spectra for sulfocoumarin in chloroform. (**d**) Representation of stokes shift between the theoretical absorption and emission spectra for sulfocoumarin in chloroform

electron-donating group. The sulfonyl, lactone and methacrylate carbonyl are electronegative, while the hydroxy group is electropositive. Terminal methyls are neutral and hydrogens attached to carbons 4 and 5 of coumarin are slightly electropositive protons.

Theoretical absorption and emission values of the SCou compound were calculated by Time-Dependent Density Functional Theory (TD-DFT) method using the Polarizable Continuum Model (PCM) in chloroform and compared with experimental values (Fig. 12). In the absorption of the SCou compound, the experimental HOMO → LUMO transition is at 343 nm and the calculated HOMO → LUMO (98%) transition is at 346 nm. In the emission of the SCou compound, the experimental HOMO → LUMO transition is at 433 nm and the calculated HOMO → LUMO transition (98%) is at 417 nm. The stokes shifts between absorption and emission are 6060 cm^{-1} (90 nm) for experimental and 4921 cm^{-1} (71 nm) for theoretical.

Dielectric properties

It is very important to investigate the dielectric behavior of newly obtained polymers for the determination of electronic components. Impedance analyzer technique is one of the most common methods used to determine the dielectric behavior of functional polymers. The dielectric constant is polarization capacity for materials in applied electrical area [55]. Dielectric properties change depending on frequency and temperature. The dielectric constant is a parameter that provides important information about the phase transitions and electron transport mechanism in polymer structures [56]. In order to determine the dielectric properties, first of all, the powder polymer was formed into a disc with a diameter of 13 mm under 5 tons of pressure. The thickness of these prepared discs was precisely measured with a digital caliper. Capacitance (Cp), loss factor (DF) and conductance (Gp) values were recorded in the range

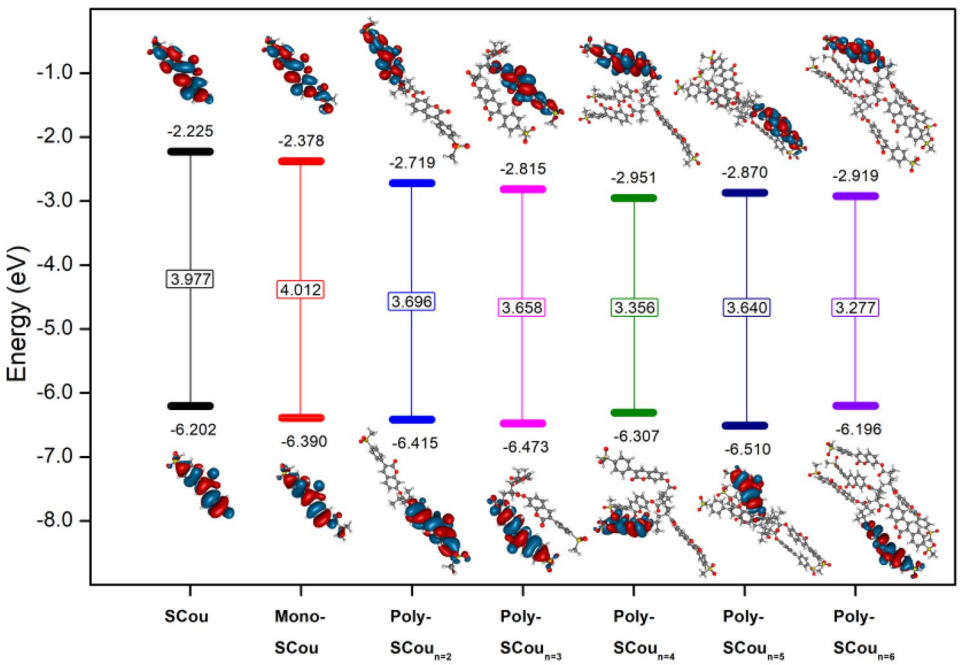

Fig. 11 The obtained molecular orbital diagram from DFT of sulfocoumarin (SCou), monomer-sulfocoumarin SCou-MA and polymer sulfocoumarins Poly(SCou$_{n=2-6}$)

of 1 kHz to 200 kHz with a computer-controlled HIOKI brand IM3536 model impedance analyzer. As a result of the results obtained, dielectric constant (ε'), dielectric loss (ε″) and conductivity (log σac) values were plotted against frequency as shown in Fig. 13.

$$\varepsilon^{'} C_p \frac{d}{A\varepsilon_0} \tag{1}$$

$$\varepsilon^{''} = \varepsilon^{'} DF \tag{2}$$

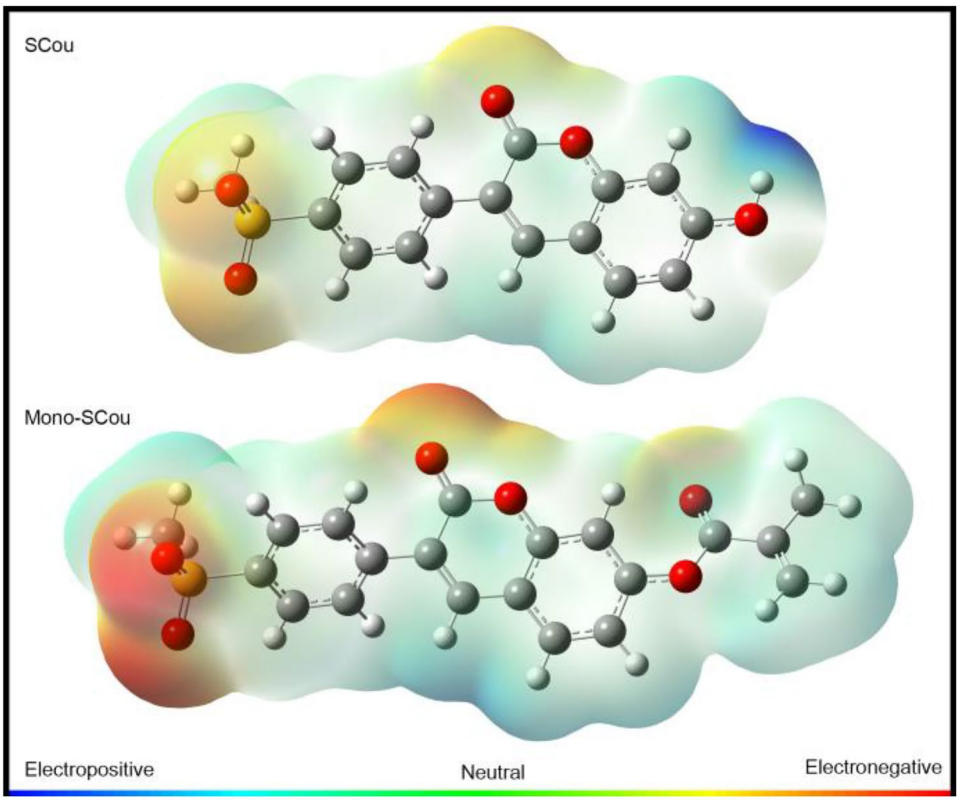

Fig. 12 Displaying and comparisoning of the electron density surfaces of sulfocoumarin (SCou) and monomer-sulfocoumarin SCou-MA

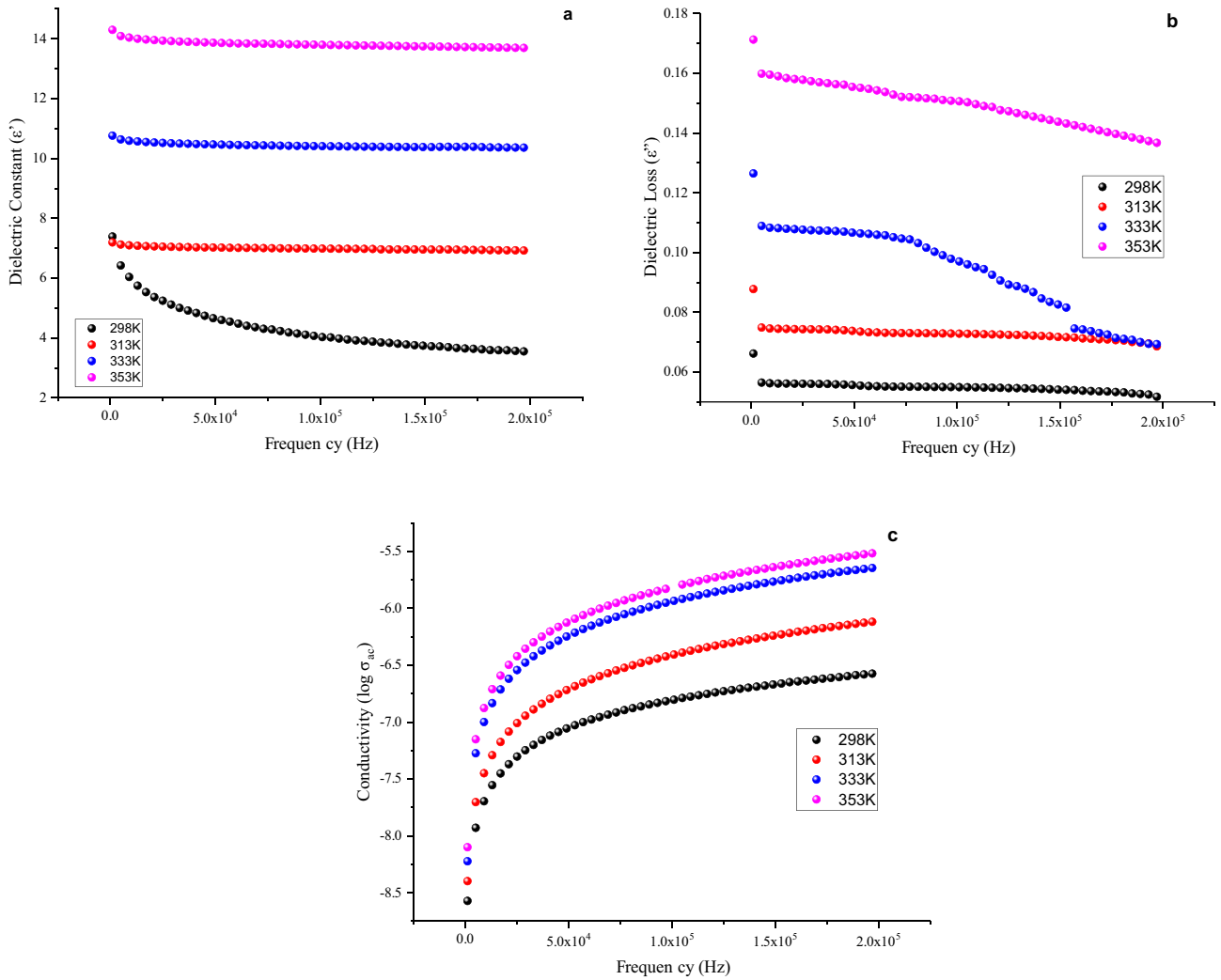

Fig. 13 Variation of (**a**) dielectric constant (**b**) dielectric loss anda (**c**) conductivity of poly (SCou)

A: surface area of the sample (m^2); ε': dielectric constant
C: parallel capacitance (F); ε″: dielectric loss
d: thickness of the polymer sample (m)
ε_0: ermittivity in free space (8.85×10^{-12} F/m)

The variation of the dielectric constant, dielectric loss and ac conductivity of the homopolymer with frequency (1–200 kHz) and temperature (25, 40, 60, 80 °C) is shown in the Fig. 13. It is clearly seen that the dielectric constant decreases with increasing frequency values at constant temperatures. It is also possible to see that the dielectric constant increases with increasing temperature values. It has been observed that the dielectric constant and dielectric loss decrease as the frequency increases and remain constant at higher frequency values [57]. The reason for this situation is that there is no interfacial polarization mechanism at high frequencies and therefore the dielectric constant at high frequencies does not show a sudden decrease as in the low frequency region [58].

A significant change was observed in the dielectric constant of the polymer with the increase in temperature. The dielectric constant increased from 6.91 to 14.02 at 1 kHz from room temperature to 80 °C. In the literature, dielectric constant of coumarin-containing polymer at 1 kHz at room temperature was determined as 5.91.

In this study dielectric constant of P(SCou) higher than the this polymer containing chlorine-coumarin [36].

Table 2 Dielectric parameters of Poly(SCou) at different temperature

Tempeture (K)	Dielectric Constant (ε')	Dielectric Loss (ε'')	AC conductivity (σ_{ac})	log σ_{ac}
298	6.91	0.0562	2.21×10^{-08}	-7.655
313	7.09	0.0745	3.94×10^{-08}	-7.404
333	10.58	0.1082	1.11×10^{-07}	-6.951
353	14.02	0.1595	1.48×10^{-07}	-6.829

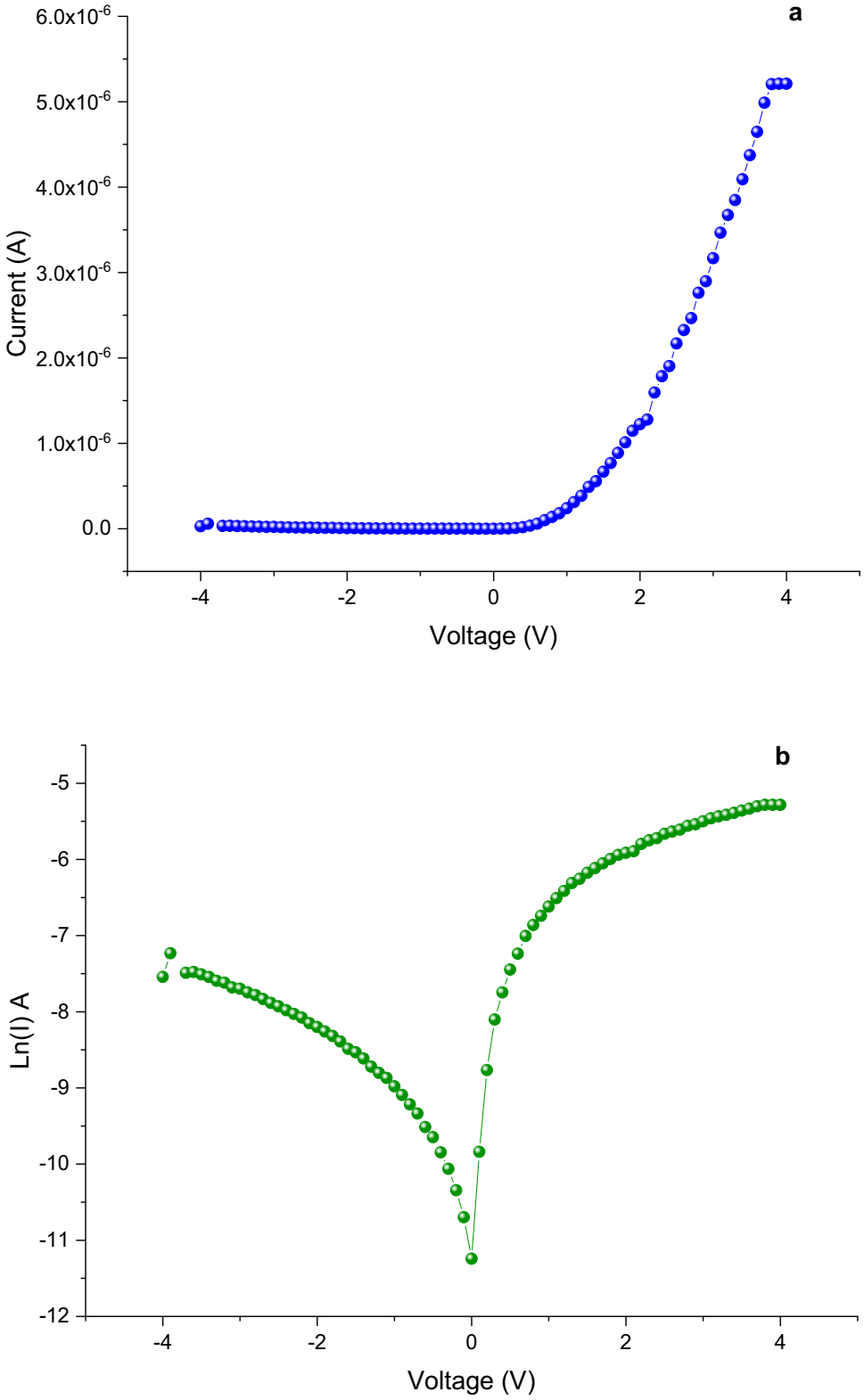

Fig. 14 **(a)** Dark characteristics of polymer composite/Si heterojunction photodiode **(b)** response of the Si/polymer composite photodiode without UV light illumination

P(SCou) contains coumarin and sulfo groups together in this structure, so it becomes more polarized in the electric field. The increase in dielectric properties with temperature can be referred to an increase in charge density as a result of interface polarization. As the temperature increases, polarization of polar groups and pi-conjugation increase the dielectric constant. The dielectric properties of the polymer increased, as the orientation of the dipoles became easier at

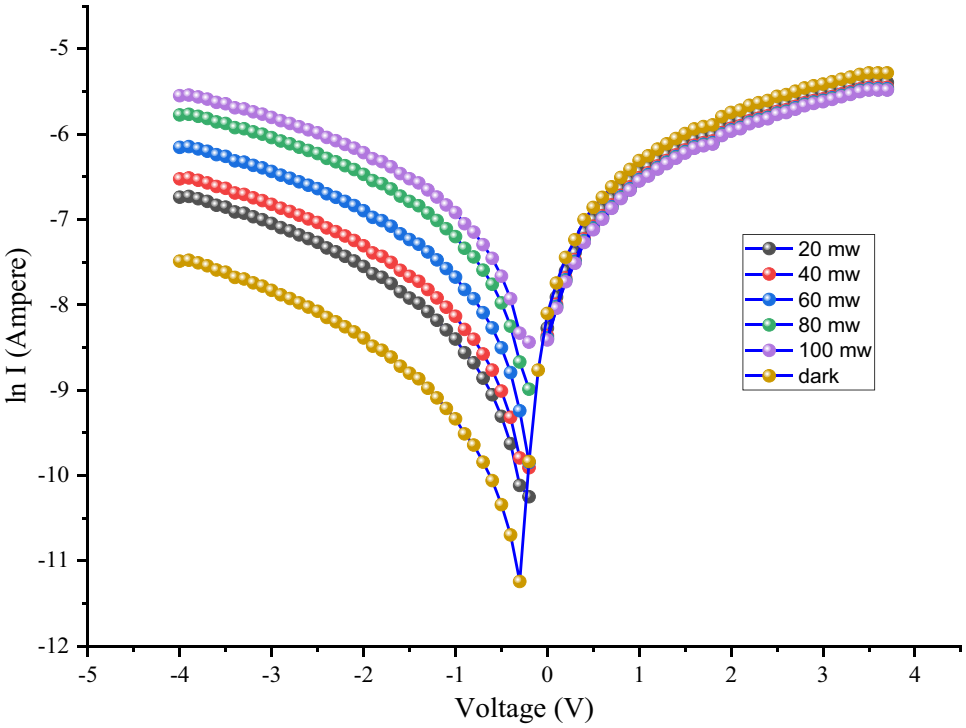

Fig. 15 The current–voltage graph of poly(SCou) photodiode under different intensities of solar light

high temperatures. In this context, from 25 °C to 80 °C the dielectric loss changed from 0.056 to 0.159, the AC conductivity changed from 2.21×10^{-8} to 1.48×10^{-7} S cm^{-1}. The dielectric parameters of P(SCou) at different temperature are summarized in Table 2.

Electrical properties

The aluminum ohmic contact p-Si substrate was cleaned in an ultrasonic homogenizer using deionized water and dried with a nitrogen gas. The polymer tetrahydrofuran was coated as a thin film on p-Si by drop coating method. The prepared films were dried on a hot plate at 40 °C. For the upper contact, aluminum was coated on the p-Si wafer. The current–voltage and capacitance–voltage measurements carried out by using FYtronic Electric Characterization system. The current–voltage characteristics of the polymer were determined using various illumination intensities between ± 4 V at room temperature. The I-V characteristics of the polymer/p-Si thin film planar heterojunction diode are shown in Fig. 14. The current–voltage characteristics of the produced diode showed good rectification behavior. The rectification ratio of the heterojunction diode in dark conditions was calculated as (RR) 86.125. While there is no significant change in the flow values in the reverse region, there is an increase in the flow in the forward region. This means that this device, which transmits electric current in one direction, can be used as a diode.

The ideality factor (n) of the diode was calculated by using Eq. 4 [59]. Where k is the boltzman constant k: 8.61×10^{-5} eV·K^{-1} where T is the analysis temperature in Kelvin.

$$n = q\, dV/kT\, ln\, (I) \tag{4}$$

According to this equation, the lnI versus V graph of the diode was drawn. The ideality factor (n) was determined using the slope of the forward current region, and also the constant value of this line equation is equal to the reverse feed saturation current ln I_0. The ideality factor was determined as 3.71 and the reverse supply current was determined as 8.78×10^{-5} A. The ideality factor provides information about the recombination process occurring in the diode and helps to compare it with an ideal diode. However, the reverse current gives the number of charge carriers that can exceed the barrier height in the reverse direction [60].

The Barrier height of the diode was calculated by using Eq. 5. Here, A* = 32 A/cm^2 K^{-2}, the effective Richardson constant for p-Si.

$$\theta = \frac{kT}{q}\, ln \left(\frac{AA^*T^2}{I_0} \right) \tag{5}$$

The barrier height is distribution in minority charge carriers between n-side and p-side of the diode and depletion region of the diode and calculated 0.54 eV for polymer/p-Si thin film planar heterojunction diode [61]. I-V behaviors at various illumination intensities of P(SCou) are shown

in Fig. 15. There are gaps between the current values in the reverse bias region in the measurements in the dark and under the light in the figure. These intervals caused an increase in the light sensitivity of the diode in reverse current with increasing illumination intensity. There are strong intervals between current values in the reverse bias zone of the performed measurements in the dark and under illumination.

Conclusion

In conclusion, new methacrylate monomer containing sulfo-coumarin group and its homopolymer were synthesized. TGA analyzes were recorded at different heating rates to determine the thermal kinetic behavior of the polymer. According to the TGA results, thermal stability increased depending on the heating rate. The average activation energy was calculated as 220 kJ/mol according to the FWO method. Theoretical calculation of compounds were done with Gaussian. Optical band gaps for SCou, SCo-MA and P(SCou) are 3.615, 3.723 and 3.792 eV, respectively.

The dielectric properties of the P(SCou) were investigated as a function of frequency and temperature in the frequency range of 1–200 kHz. It is clearly seen that the dielectric constant decreases with increasing frequency at constant temperatures. The reason for this situation is that there is no interfacial polarization mechanism at high frequencies and therefore the dielectric constant at high frequencies does not show a sudden decrease as in the low frequency region. A significant change was observed in the dielectric constant of the polymer with the increase in temperature. The dielectric constant increased from 3.81 to 14.02 at 1 kHz from room temperature to 80 °C. The increase in dielectric properties with temperature can be referred to an increase in charge density as a result of interface polarization.

The current–voltage characteristics of the polymer were determined using various illumination intensities between ± 4 V at room temperature. The current–voltage characteristics of the produced diode showed good rectification behavior. The rectification ratio of the heterojunction diode in dark conditions was calculated as 86.125. The ideality factor was determined as 3.71, and the reverse supply current was determined as 8.78×10^{-5} A. The ideality factor provides information about the recombination process occurring in the diode and helps to compare it with an ideal diode. According to the results, the properties of the P(SCou)/pSi diode produced can be used in photodiode and sensor technology applications.

Declarations

Conflict of Interest There is a conflict of interest with Prof. Dr. Kadir Demirelli.

References

1. Kunkel C, Margraf JT, Chen K, Oberhofer H, Reuter K (2021) Active discovery of organic semiconductors. Nat Commun 12:1–11
2. Mishra A, Bäuerle P (2012) Small molecule organic semiconductors on the move: promises for future solar energy technology. Angew Chem Int Ed 51:2020–2067
3. Tombak A, Ocak YS, Asubay S, Kilicoglu T, Ozkahraman F (2014) Fabrication and electrical properties of an organic–inorganic device based on Coumarin 30 dye. Mater Sci Semicond Process 24:187–192
4. Reddy MSP, Lee J-H, Jang J-S (2013) Frequency dependent series resistance and interface states in Au/bio-organic/n-GaN Schottky structures based on DNA biopolymer. Synth Met 185:167–171
5. Demirezen S, Yerişkin SA (2020) A detailed comparative study on electrical and photovoltaic characteristics of Al/p-Si photodiodes with coumarin-doped PVA interfacial layer: the effect of doping concentration. Polym Bull 77:49–71
6. Tan SO, Tecimer H, Cicek O (2017) Comparative investigation on the effects of organic and inorganic interlayers in Au/n-GaAs Schottky diodes. IEEE Trans Electron Devices 64:984–990
7. Piller N (1997) Mode of action of coumarin in the treatment of thermal injuries. Coumarins: Biology, Applications and Mode of Action: John Wiley & Sons Ltd. 185–208
8. Essaïdi Z, Krupka O, Iliopoulos K, Champigny E, Sahraoui B, Sallé M et al (2013) Synthesis and functionalization of coumarin-containing copolymers for second order optical nonlinearities. Opt Mater 35:576–581
9. Abdou MM, El-Saeed RA, Bondock S (2019) Recent advances in 4-hydroxycoumarin chemistry. Part 1: Synthesis and reactions. Arabian J Chem 12:88–121
10. Abdou MM, El-Saeed RA, Bondock S (2019) Recent advances in 4-hydroxycoumarin chemistry. Part 2: Scaffolds for heterocycle molecular diversity. Arabian J Chem 12:974–1003.
11. Abdou MM (2017) 3-Acetyl-4-hydroxycoumarin: Synthesis, reactions and applications. Arab J Chem 10:S3664–S3675
12. Yazdanbakhsh M, Ghanadzadeh A, Moradi E (2007) Synthesis of some new azo dyes derived from 4-hydroxy coumarin and spectrometric determination of their acidic dissociation constants. J Mol Liq 136:165–168
13. Aslan F, Esen H, Yakuphanoglu F (2020) Al/P-Si/Coumarin: TiO 2/Al organic-inorganic hybrid photodiodes: investigation of electrical and structural properties. SILICON 12:2149–2164
14. Mir FA, u Rehman S, Asokan K, Khan S, Bhat G (2014) Optical, DC and AC electrical investigations of 4-hydroxy coumarin molecule as an organic Schottky diode. J Mater Sci: Mater Electron 25:1258–63
15. Liu X, Cole JM, Waddell PG, Lin T-C, Radia J, Zeidler A (2012) Molecular origins of optoelectronic properties in coumarin dyes: toward designer solar cell and laser applications. J Phys Chem A 116:727–737
16. Nian L, Zhang W, Zhu N, Liu L, Xie Z, Wu H et al (2015) Photoconductive cathode interlayer for highly efficient inverted polymer solar cells. J Am Chem Soc 137:6995–6998

17. Zhang H, Yu T, Zhao Y, Fan D, Qian L, Yang C et al (2007) Syntheses, characterization and fluorescent properties of two triethylene-glycol dicoumarin-3-carboxylates. Spectrochim Acta Part A Mol Biomol Spectrosc 68:725–727
18. Tathe AB, Sekar N (2016) Red emitting coumarin—azo dyes: synthesis, characterization, linear and non-linear optical properties-experimental and computational approach. J Fluoresc 26:1279–1293
19. Makhlouf M, Zeyada H (2016) Synthesis, structural analysis, spectrophotometric measurements and semiconducting properties of 3-phenyl azo-4-hydroxycoumarin thin films. Synth Met 211:1–13
20. Yadav N, Singh S, Mangawa SK, Dixit SK, Gupta U, Khajuria Y et al (2015) Fluorescent probe 7-(prop-2-yn-1-yloxy)-2H-chromen-2-one: Experimental and DFT based approach to photophysical properties. Spectrochim Acta Part A Mol Biomol Spectrosc 148:311–317
21. Mishra A, Fischer MK, Bäuerle P (2009) Metal-free organic dyes for dye-sensitized solar cells: From structure: Property relationships to design rules. Angew Chem Int Ed 48:2474–2499
22. Soykan C, Erol I, Kirbag S (2003) Synthesis and characterization of poly(1,3-thiazol-2-yl-carbomoyl) methyl methacrylate: Its metal complexes and antimicrobial activity studies. J Appl Polym Sci 90:3244–3251
23. Erol I, Akbıyık, H Kinetic parameters, thermal stability, biological activity, and dielectric properties of new methacrylate-based copolymers functionalized with methylparaben. J Polym Res 22;29:1–21
24. Zhang W, Tu Z, Qian J, Choudhury S, Archer LA, Lu Y (2018) Design principles of functional polymer separators for high-energy, metal-based batteries. Small 14:1703001
25. Chen L, Yan C, Zheng Z (2018) Functional polymer surfaces for controlling cell behaviors. Mater Today 21:38–59
26. MacFarlane LR, Shaikh H, Garcia-Hernandez JD, Vespa M, Fukui T, Manners I (2021) Functional nanoparticles through π-conjugated polymer self-assembly. Nat Rev Mater 6:7–26
27. Liu F, Zhang J, Zhou Z, Zhang J, Wei Z, Zhu X (2017) Poly (3-hexylthiophene)-based non-fullerene solar cells achieve high photovoltaic performance with small energy loss. J Mater Chem A 5:16573–16579
28. Lin Y, Li T, Zhao F, Han L, Wang Z, Wu Y et al (2016) Structure Evolution of Oligomer Fused-Ring Electron Acceptors toward High Efficiency of As-Cast Polymer Solar Cells. Adv Energy Mater 6:1600854
29. Nicholson J, Brookman P, Lacy O, Sayers G, Wilson A (1988) A study of the nature and formation of zinc polyacrylate cement using Fourier transform infrared spectroscopy. J Biomed Mater Res 22:623–631
30. Grigoras M, Catanescu CO (2004) Imine oligomers and polymers. J Macromole Sci Part C: Polym Rev 44:131–173
31. Jenekhe SA, Yang CJ, Vanherzeele H, Meth JS (1991) Cubic nonlinear optics of polymer thin films. Effects of structure and dispersion on the nonlinear optical properties of aromatic Schiff base polymers. Chem Mater 3:985–7
32. Çaykara T, Özyürek C, Kantoğlu Ö, Erdoğan B (2003) Thermal behavior of poly(2-hydroxyethyl methacrylate-maleic acid) networks. Polym Degrad Stab 80:339–343
33. Abubakar AM, Biryan F, Demirelli K (2019) Electrical properties, characterization, and preparation of composite materials containing a polymethacrylate with α-naphthyl side group and nanographene fillers. J Thermoplast Compos Mater 34:102–125
34. Šimon P (2004) Isoconversional methods. J Therm Anal Calorim 76:123–132
35. Flynn JH, Wall LA (1966) General treatment of the thermogravimetry of polymers. J Res Natl Bureau Standards Sect A. Phys Chem 70:487
36. Biryan F, Pihtili G, Demirelli K (2020) Thermal studies and influence of the thermal decomposition on dielectric properties of a new coumarin copolymers. J Therm Anal Calorim 139:3871–3885
37. Biryan F, Demirelli K (2019) Thermal degradation kinetic, electrical and dielectric behavior of brush copolymer with a polystyrene backbone and polyacrylate-amide side chains/nanographene-filled composites. J Mol Struct 1186:187–203
38. Gupta GK, Mondal MK (2019) Kinetics and thermodynamic analysis of maize cob pyrolysis for its bioenergy potential using thermogravimetric analyzer. J Therm Anal Calorim 137:1431–1441
39. Acquah C, Danquah MK, Moy CK, Anwar M, Ongkudon CM (2017) Thermogravimetric characterization of ex situ polymethacrylate (EDMA-co-GMA) monoliths. Canadian J Chem Eng 95:1345–1351
40. Caricato M, Vreven T, Trucks GW, Frisch MJ, Wiberg KB (2009) Using the ONIOM hybrid method to apply equation of motion CCSD to larger systems: Benchmarking and comparison with time-dependent density functional theory, configuration interaction singles, and time-dependent Hartree-Fock. J Chem Phys 131:10B604
41. Dennington R, Keith, T, Millam J (2009) Gauss View. Version 5 Semichem Inc Shawnee Mission.
42. Becke AD (1988) Density-functional exchange-energy approximation with correct asymptotic behavior. Phys Rev A 38:3098
43. Becke AD (1993) Density-functional thermochemistry. III. The role of exact exchange. J Chem Phys 98:5648–52
44. Lee C, Yang W, Parr RG (1988) Development of the Colle-Salvetti correlation-energy formula into a functional of the electron density. Phys Rev B 37:785
45. Tomasi J, Mennucci B, Cancès E (1999) The IEF version of the PCM solvation method: an overview of a new method addressed to study molecular solutes at the QM ab initio level. J Mol Struct (Thoechem) 464:211–226
46. Tomasi J, Mennucci B, Cammi R (2005) Quantum mechanical continuum solvation models. Chem Rev 105:2999–3094
47. Behera B, Das PK (2018) Blue- and Red-Shifting Hydrogen Bonding: A Gas Phase FTIR and Ab Initio Study of RR′CO···DCCl3 and RR′S···DCCl3 Complexes. J Phys Chem A 122:4481–4489
48. Koopmans T (1934) Über die Zuordnung von Wellenfunktionen und Eigenwerten zu den Einzelnen Elektronen Eines Atoms. Physica 1:104–113
49. Mulliken RS (1934) A New Electroaffinity Scale; Together with Data on Valence States and on Valence Ionization Potentials and Electron Affinities. J Chem Phys 2:782–793
50. Pearson RG (1987) Recent advances in the concept of hard and soft acids and bases. J Chem Educ 64:561
51. Parr RG, Chattaraj PK (1991) Principle of maximum hardness. J Am Chem Soc 113:1854–1855
52. Parr RG, Pearson RG (1983) Absolute hardness: companion parameter to absolute electronegativity. J Am Chem Soc 105:7512–7516
53. Parr RG, Szentpály Lv, Liu S (1999) Electrophilicity Index. J Am Chem Soc 121:1922–4
54. Padmanabhan J, Parthasarathi R, Subramanian V, Chattaraj PK (2007) Electrophilicity-Based Charge Transfer Descriptor. J Phys Chem A 111:1358–1361
55. Zheng W, Wong S-C (2003) Electrical conductivity and dielectric properties of PMMA/expanded graphite composites. Compos Sci Technol 63:225–235
56. Bal KK, V K(2009) Measurement of dielectric properties of textile materials and their applications. Ind J Fıbre Tex Res 191–9
57. Beladakere NN, Misra SCK, Ram MK, Rout DK, Gupta R, Malhotra BD et al (1992) Interfacial polarization in semiconducting polypyrrole thin films. J Phys: Condens Matter 4:5747–5756
58. Vickers NJ (2017) Animal Communication: When I'm Calling You, Will You Answer Too? Curr Biol 27:R713–R715

59. Çiçek O, Tecimer HU, Tan SO, Tecimer H, Altındal Ş, Uslu İ (2016) Evaluation of electrical and photovoltaic behaviours as comparative of Au/n-GaAs (MS) diodes with and without pure and graphene (Gr)-doped polyvinyl alcohol (PVA) interfacial layer under dark and illuminated conditions. Compos B Eng 98:260–268
60. Sharma GD, Saxena D, Roy MS (2004) Dark, photoelectrical properties and impedance analysis of organic semiconductor based donor/acceptor device. Thin Solid Films 467:220–226
61. Gozeh BA, Karabulut A, Ismael CB, Saleh SI, Yakuphanoglu F (2021) Zn-doped CdO effects on the optical, electrical and photoresponse properties of heterojunctions-based photodiodes. J Alloy Compd 872:159624